Impact of Environmental Conditions on Grass Phenology in the Regional Climate Model COSMO-CLM

Eva Nowatzki[1], Jan-Peter Schulz[2], Ruben Seibert[3], Marius Schmidt[4], Mingyue Zhang[1], Jürg Luterbacher[1,5], and Merja Tölle[1]

[1]Department of Geography, Climatology, Climate Dynamics and Climate Change, Justus-Liebig University Giessen, Giessen, Germany
[2]Deutscher Wetterdienst (DWD, German Meteorological Service), Offenbach, Germany
[3]Department of Biology, Plant Ecology, Justus-Liebig University Giessen, Giessen, Germany
[4]Institute of Bio- and Geosciences, Agrosphere (IBG-3), Forschungszentrum Jülich, Jülich, Germany
[5]World Meteorological Organization (WMO), Science and Innovation Department, Geneva, Switzerland

Key Points:

- COSMO-CLM simulations with phenology depending on surface temperature, day length, and water availability show a significant improvement of the mean annual cycle of LAI in experiments over Germany covering the period 1999-2015.
- Years with an extremely warm winter/spring or an extremely dry summer affect interannual variations of LAI with an earlier start of the growing season or reduced LAI due to lack of water in the simulations with the new phenology in very good agreement with the observations.
- Changes in LAI of grass influence the number of extreme hot/wet days and the transpiration rate, resulting in enhanced simulated latent heat flux.

Corresponding author: Eva Nowatzki, eva.nowatzki@geogr.uni-giessen.de

Abstract

Phenology and its interannual variability are altered through anthropogenic climate change. Feedbacks of plant phenology to the regional climate system affect fluxes of energy, water, CO2, biogenic volatile organic compounds as well as canopy conductance, surface roughness length, and are influencing the seasonality of albedo. We performed simulations with the regional climate model COSMO-CLM (CCLM) with 3 km horizontal resolution over Germany covering the period 1999 to 2015 to study the sensitivity of grass phenology to different environmental conditions by implementing a new phenology module. We provide new evidence that the standard annually-recurring phenology of CCLM is improved by the new calculation of leaf area index (LAI) dependent upon surface temperature, day length, and water availability. Results with the new phenology implemented in the model showed a significantly higher correlation with observations than simulations with the standard phenology. The interannual variability of LAI, the representation of years with extremely warm spring or extremely dry summer, and the start of the growing season also improved with the new phenology module. The number of hot days with maximum temperature exceeding the 90th percentile and heavy precipitation events ($>$ 20 mm) with the new phenology are in very good agreement with the observations. We also show that lower LAI values in summer lead to a decrease of latent heat flux in the model due to less evapotranspiration. The CCLM simulation with improved representation of the phenology should be used in future applications with an extension on more plant functional types.

1 Introduction

Phenology is the timing of seasonal activities of animals and plants (Schnelle, 1955; Walther et al., 2002). It indicates changes in ecology (Walther et al., 2002) which are linked to local or regional climate variability (Parmesan, 2006). Phenology is also affected by climate change (Parmesan & Yohe, 2003; Settele et al., 2014), since the 1950s, the growing season in temperate Europe lengthened by 3.6 days per decade (Menzel & Fabian, 1999; Walther et al., 2002; Jeong et al., 2011). With higher CO_2 concentrations and warmer conditions, the growing season will further extend (Reyes-Fox et al., 2014).

The phenology mainly depends on the vegetation type, but also temperature and precipitation influence the phenological stages (White et al., 1997). Additionally, the length of the photoperiod (day length) plays an important role, and together with temperature influences the length of the growing period (Heide, 1974; Oleksyn et al., 1992). The precipitation and the available soil water are important for the variability during the phenophase (Hodges, 1991). Years with an exceptional course of phenology are also associated with extreme temperature and/or precipitation (Shen et al., 2011). When a year starts with an anomalous warm winter and spring, the vegetation usually also starts growing earlier, and later when winter/spring is cold. The end of the growing season is usually earlier when the late summer or autumn is colder than usual, and later when it is warm (Chmielewski & Rötzer, 2002). Precipitation as a source for soil water has a strong influence on the development of the leaf area index (LAI, the leaf area per unit area of land (Watson, 1947)) especially in summer during the growing season (Currie & Peterson, 1966). The more precipitation occurs the more water is available for the plants. In a year with less precipitation, there is less water available thus a reduction of the LAI is observed (Gilgen & Buchmann, 2009).

Inversely, the energy and water cycle of the regional climate is influenced by the phenological development of the vegetation through albedo, and sensible and latent heat flux changes (Peñuelas et al., 2009). This influences near-surface air temperature, precipitation, and ultimately the boundary layer structure. The impact of vegetation on the weather and climate conditions (Collatz et al., 2000; Tölle et al., 2014) are most visible in extreme events as the 2003 European summer heatwaves (Stéfanon et al., 2012). Higher insolation in spring enhances evapotranspiration in June leading to land surface cooling, whereas in August the evapotranspiration is reduced by water stress leading to an

early leave fall (Stéfanon et al., 2012). The sensitivity of latent heat flux to vegetation is shown in Yang et al. (1999); Peñuelas et al. (2009); I. N. Williams and Torn (2015) and is already validated for different land-surface models (Flerchinger et al., 1998; Nagai, 2003; Best & Grimmond, 2016).

Phenology and associated vegetation dynamics are accounted for in many different land surface models and still need improvements (Richardson et al., 2013). Main examples are the Community-Land Model (CLM) (Oleson et al., 2013), the Lund-Potsdam-Jena (LPJ) (Sitch et al., 2003) and ORCHIDEE (Ryder et al., 2014). These sophisticated land surface models are coupled to many regional climate models. The computational costs are very high and the horizontal resolution of the grid is rather coarse ($\sim 12-50\,\mathrm{km}$). High horizontal resolution ($\sim 1-3\,\mathrm{km}$) and less computational demand can be achieved through less complex models. For example, the regional climate model COSMO-CLM (CCLM) is used for applications at a convection-permitting scale with the land surface model TERRA-ML (Doms et al., 2011; Schulz et al., 2016). It is a land-surface model of the second generation using the so-called BATS model (Dickinson, 1984) or the simpler Bucket model (Manabe, 1969). In CCLM, the phenology is static and does not depend on the environmental conditions. It follows a sinusoidal cycle depending on the geographical latitude and altitude (Doms et al., 2011; Schättler & Blahak, 2017). Because those are constants, the annual cycle is every year the same for each simulated location. The annual cycle of LAI starts with the growth of the vegetation in spring and ends with the senescence in autumn. Those events differ from year to year in nature and should therefore also in the model do so. Vegetation-atmosphere interactions need to be accurately represented in regional climate models to improve projections. The static annually-recurring phenology is in contradiction to the changing phenological cycle due to climate change that is observed. The CCLM is neither able to simulate the interannual variability of vegetation nor the feedbacks between climate and vegetation. Therefore, the model needs to be improved through phenology susceptible to environmental conditions. Models calculating phenology based on temperature give better results compared to satellite observations than models with complex photosynthetic modules (Murray-Tortarolo et al., 2013). That is why a calculation of phenology based on temperature is chosen (Knorr et al., 2010).

The main objective of this study is to implement a new phenology calculation for grassland in the CCLM model. The new phenology depends on the surface temperature, the day length, and the water availability, allowing for interannual variability of the LAI. We will examine three experimental areas in Germany from 1999 to 2015. The simulated mean annual cycle and the annual cycle of extreme years of LAI will be compared to observations. Further, the influence of phenology on extreme events of temperature and precipitation will be studied. Additionally, the impact of the phenology on the latent heat flux in the CCLM model will be evaluated in this study. To assess the performance of this new phenology, the following research questions will be addressed:

1. How is the annual cycle of LAI affected by the newly implemented phenology?
2. Does the representation of extreme events in CCLM change with the new phenology module?
3. What is the influence of the phenology on atmospheric variables, such as temperature, precipitation, and moisture?

2 Data and Methods

2.1 Meteorological Observations

The three experimental domains are chosen to be at locations with observational sites (figure 1). The Lindenberg Meteorological Observatory (station ID 03015) is operated by the German Meteorological Service (Deutscher Wetterdienst, DWD) (Neisser et al., 2002). Temperature and precipitation data are freely available. At Linden is the mea-

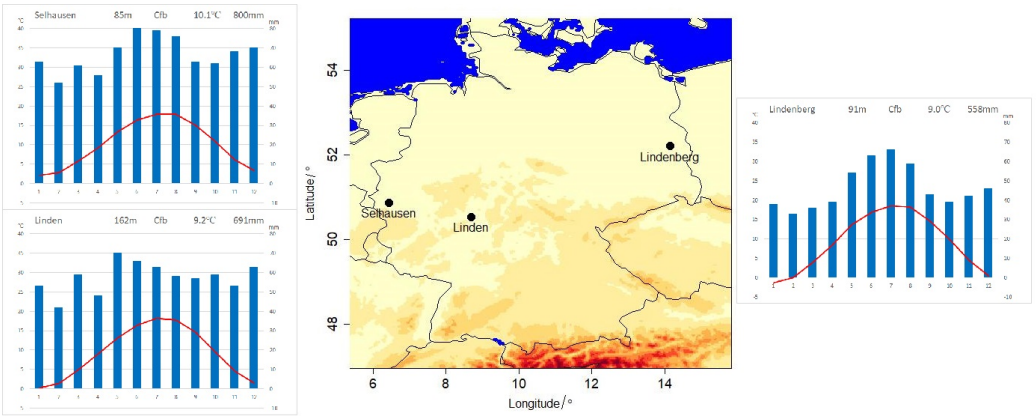

Figure 1. The map with the three experimental locations (Lindenberg, Linden, and Selhausen) surrounded by their climate diagrams (data from Merkel (2020), 1982-2012).

suring station of the University of Giessen for the GiFACE project (Jäger et al., 2003; Andresen et al., 2018). Besides the meteorological measurements of temperature and precipitation, leaf area index measurements are available for individual years. The experimental crop site of Selhausen is operated by the Institute of Bio- and Geosciences, Agrosphere (IBG-3) of the Forschungszentrum Jülich (Post et al., 2018; Bogena et al., 2018). Measurements of leaf area index and air temperature from the site were available at the CRC/TR32 database (https://www.tr32db.uni-koeln.de) or the TERENO data portal (http://www.tereno.net/ddp/). In addition, precipitation data from the DWD station Jülich (02473) is included. The station data will be used to find extremely warm/dry years.

Precipitation and temperature information is also taken from HYRAS, a high-resolution gridded daily data set with 5 km spatial and a daily temporal resolution (Rauthe et al., 2013). The HYRAS data set is calculated from the information of approximately 6200 stations including the DWD stations using the REGNIE method, a combination of multiple linear regression considering orographical conditions and inverse distance weighting (Rauthe et al., 2013). This daily gridded data set will be used to derive heavy precipitation and hot temperature events. The threshold for heavy precipitation amount at a certain time is set to 20 mm per day (Kundzewicz et al., 2006; Bartholy & Pongrácz, 2007). An extremely hot day is defined as a day within the 90 th percentile of maximum temperature (Yan et al., 2002; González-Aparicio & Hidalgo, 2012).

2.2 LAI Measurements

Indirect methods based on radiation measurements are applied to measure the LAI. The indirect method is not as precise as the direct method (collect leaves and measure their area) but can easily be automated and is less expensive and complex (Cutini et al., 1998). One of the common indirect methods is the plant canopy analyzer LAI-2000 (Li-Cor, 1992) or the SunScan SS1 LAI meter (Delta-T Devices Ltd, Cambridge, UK). Here LAI is determined by measuring the light extinction in a canopy that is related to LAI. The indirect method is used at Linden and Selhausen to obtain the leaf area index. The measurements are made over grassland covering an area of about 100 m x 200 m in Linden from 1998 to 2002 (Kammann et al., 2005) and from 2014 to 2016 and in Selhausen from 2016 to 2018 over crops (2016: barley followed by greening mix, 2017: sugar beet, 2018: winter wheat).

We also use satellite observed leaf area index data because in-situ measurements are very sparse regarding spatial and temporal resolution. The LAI is calculated from

the satellite product of SPOT and PROBA-V (Smets et al., 2019), derived from the normalized reflectance of red, near-infrared, and shortwave-infrared radiation (Verger et al., 2014). Because the vegetation is not equally distributed in reality it comes to an irregular distribution of the plants within remote sensing products (clumping). Therefore, this product uses a method to distribute the vegetation equally in the resolved grid (Chen et al., 2005). The data is provided by the University of Hamburg with a horizontal resolution of 1 km and a temporal resolution of 10 days from 1999 to 2015 (Baret et al., 2013; Camacho et al., 2013). For comparison with the simulations, one grid cell of the gridded leaf area index will be used at each experimental domain. One pixel of the satellite data is 50 times larger than the area of the in-situ measurements. This means that there is not only grass in this pixel but also other vegetation types including forests and crops and non-vegetated surfaces (urban areas). The LAI measurements from the FACE (Jäger et al., 2003; Andresen et al., 2018) and the Tereno project (Post et al., 2018; Bogena et al., 2018) will be used to validate the satellite observations at the two specific areas because in-situ measurements of LAI have much more precise results at a specific location but cover a limited area and time. The satellite observations will finally be used to evaluate the simulations at the three locations and for the whole period.

2.3 COSMO-CLM

The simulations will be performed with the regional climate model COSMO-CLM (Rockel et al., 2008) in single column mode. COSMO-CLM is the model of the COnsortium for Small-scale MOdelling (COSMO) in CLimate Mode (Baldauf et al., 2011; Rockel et al., 2008) and is the community model of the German regional climate research community jointly further developed by the CLM-Community. The COSMO model version 5.0 with CLM version 15 (COSMO-CLM − $v5.0\_clm15$) is used. The Interpolation is done with INT2LM in version 2.05 with CLM version 1 (INT2LM−$v2.05\_clm1$) (Schättler & Blahak, 2017). The time-integration is the two time-level Runge-Kutta scheme (Jameson et al., 1981) and the model time step is 25 seconds. Following convection-permitting simulations in general, only the shallow convection parameterization based on the Tiedtke scheme (Tiedtke, 1988) is used. The land surface model is TERRA-ML (Doms et al., 2011; Schulz et al., 2016). It is a multi-layer scheme that computes temperature and water content on 10 soil layers. The bare soil evaporation and the transpiration by plants are simulated following the BATS scheme (Dickinson, 1984), together they form the evapotranspiration. The transpiration is based on a Jarvis (1976)-type formulation depending on several environmental stress factors, taking into account the LAI. The simulations are forced with ERA-Interim reanalysis data (Dee et al., 2011). The leaf area index, root depth, and vegetation area fraction in the external data file are adjusted to grassland. In this way, the simulations can be compared without being influenced by differences in land coverage.

The horizontal resolution of the simulations will be 0.0275 °, which is about 3 km. Three specific experimental domains are chosen, depending on the location of the observational sites in Germany. Those are Lindenberg ($Lat = 52.220\,°$, $Lon = 14.135\,°$, $Alt = 91\,\mathrm{m}$) in Brandenburg, Linden ($Lat = 50.531\,°$, $Lon = 8.704\,°$, $Alt = 162\,\mathrm{m}$) close to Giessen in Hesse and Selhausen ($Lat = 50.855\,°$, $Lon = 6.439\,°$, $Alt = 85\,\mathrm{m}$) close to Jülich in North Rhine-Westphalia (figure 1). At each of these domains, simulations with 25 x 25 grid points will be performed where the central grid point including the observational site is cut with all vertical layers. Each domain will be simulated from 1999 to 2015.

2.4 Implementation of the Phenology Scheme

A general logistic approach for annually changing phenology in CCLM is adapted from the LPJ philosophy of the Lund-Potsdam-Jena Dynamic Global Vegetation Model

Table 1. Parameters of the newly implemented phenology model based on Knorr et al. (2010).

Symbol	Description	Units
Λ	leaf area index	-
$t, \Delta t$	time, time step	s
r, p	growth rate, shedding rate	days^{-1}
T_S	soil surface temperature	°C
τ_m	averaging time for temperature	s
T, T_{on}	phenology temperature, threshold	°C
Λ_T	LAI depending on temperature (and day length)	-
φ	latitude	rad
δ	declination of the sun	rad
t_d, t_{on}	day length, threshold	h (hours)
W_c, W_{max}	water content, maximum available	m
τ_s	averaging time for water availability	s
Λ_W	LAI with water dependence	-
Λ_S	LAI with smoothed water availability	-

(LPJ-DGVM) (Sitch et al., 2003; Smith et al., 2001) in the form

$$\frac{d\Lambda}{dt} = r\Lambda(1 - \frac{\Lambda}{\Lambda_{max}}) - p\Lambda\,, \tag{1}$$

where LAI is Λ and its maximum value is Λ_{max}, the growth rate is r and the shedding rate is p. It is used in the LPJ as well as in JSBACH (Raddatz et al., 2007; Reick et al., 2013). The latter is the component for land and vegetation of the MPI Earth System Model (Giorgetta et al., 2013). The MPI regional climate model REMO-iMOVE (Jacob & Podzun, 1997; Wilhelm et al., 2013), a new model version with dynamic vegetation phenology of REMO, also uses this approach. We adapt the new phenology model for grassland in CCLM based on the work by Knorr et al. (2010) and the developments by Schulz et al. (2015).

All parameters used in the following equations are described in table 1 and min/max are minimum and maximum values. To avoid leaf area indices higher than the maximum values or lower than the minimum values, the higher or lower values are corrected to the limitations given by the external data. The equations are implemented in the source code of CCLM as a new module step-by-step starting with the dependence on temperature, followed by the dependence on day length, and followed by the dependence on water availability. The new module is called prior to the land surface model TERRA-ML during the model run of CCLM. In this way, the transpiration and all other influenced parameters are calculated with the new LAI.

2.4.1 Dependence on Temperature

The first step is to implement the phenology depending exclusively on the temperature. The air and surface temperature can change very fast but the vegetation needs its time to react. Therefore, a phenology determining temperature T is introduced (Knorr et al., 2010). It is defined as a temperature T depending on the soil surface temperature T_S of a past period, weighted exponentially (Knorr et al., 2010):

$$T(t + \Delta t) = T(t) \cdot e^{-\Delta t/\tau_m} + T_S(t) \cdot (1 - e^{-\Delta t/\tau_m})\,. \tag{2}$$

Following the work by Schulz et al. (2015) the past period is chosen to be $\tau_m = 15\,\text{days}$. Now the leaf area index Λ_T depending on the temperature can be calculated as follows:

$$\Lambda_T(t + \Delta t) = \begin{cases} \Lambda_{max} - e^{-r\Delta t} \cdot (\Lambda_{max} - \Lambda_T(t)), & \text{if } T \geq T_{on} \\ \Lambda_{min} - e^{-r\Delta t} \cdot (\Lambda_{min} - \Lambda_T(t)), & \text{else} \end{cases}\,, \tag{3}$$

where the growth rate is chosen to be $r = 0.07\,\text{days}^{-1}$ which is an empirically tuned value and the shedding rate is the same $p = r$ (Schulz et al., 2015). The results of simulations with this implementation are in the following denoted as $'\_T'$. The threshold of the temperature is commonly set to 0 or 5 °C (Piao et al., 2015). Following again Schulz et al. (2015) it is set to $T_{on} = 5\,°\text{C}$.

2.4.2 Dependence on Day Length

The day length at a specific location contributes to the timing of vegetation growth and decay. The day length depends on the latitude φ and the declination δ of the sun. It is calculated as

$$t_d = \arccos(-\tan\varphi \cdot \tan\delta) \cdot 24\,\text{h}/\pi\,, \tag{4}$$

and is given in hours. Now the leaf area index Λ_T depending on the temperature and the day length calculates as

$$\Lambda_T(t+\Delta t) = \begin{cases} \Lambda_{max} - e^{-r\Delta t} \cdot (\Lambda_{max} - \Lambda_T(t)), & \text{if } T \geq T_{on} \text{ and } t_d \geq t_{on} \\ \Lambda_{min} - e^{-r\Delta t} \cdot (\Lambda_{min} - \Lambda_T(t)), & \text{else} \end{cases}\,. \tag{5}$$

To have a Central European growing period which lasts at the most from February to October the threshold for the day length is set to $t_{on} = 10\,\text{h}$. The results of simulations with this implementation are denoted as $'\_TD'$.

2.4.3 Dependence on Water Availability

The water available for the plant is mainly determined by the water content of the soil. It influences the transpiration by plants (Gardner & Ehlig, 1963). The water availability is even more important for plant growth than the temperature (Woodward, 1987). Therefore, water availability has to affect the LAI in the model appropriately. The water availability is adapted from the Knorr et al. (2010) approach to the CCLM.

The water available for the plants is the soil water that can be reached with the roots. This is calculated in the model using all soil layers within the root depth of the vegetation and is called water content W_c. The maximum for the plant available water content W_{max} is also needed to obtain the ratio of available to maximum water content. It can be calculated as the difference between the field capacity $FCAP$ and the permanent wilting point PWP. With the help of these variables a water-dependent leaf area index Λ_W is calculated with

$$\Lambda_W = \Lambda_T \cdot \frac{W_c}{W_{max}}\,. \tag{6}$$

This is implemented in the model through a smoothed minimum function (Knorr et al., 2010):

$$\Lambda_S = \frac{\Lambda_T + \Lambda_W - \sqrt{(\Lambda_T + \Lambda_W)^2 - 4\eta\Lambda_T\Lambda_W}}{2\eta}\,, \tag{7}$$

where Λ_S is the smoothed water available leaf area index and $\eta = 0.99$. Finally, these steps are combined with the equation of the dependence on temperature and day length. The following equation gives the complete formulation of the leaf area index Λ depending on the temperature, the day length, and the water availability:

$$\Lambda(t+\Delta t) = \Lambda_T \cdot e^{-\Delta t/\tau_s} + \Lambda_S \cdot (1 - e^{-\Delta t/\tau_s})\,. \tag{8}$$

Results of simulations with all parts of the new phenology implemented are denoted as $'\_TDW'$.

3 Results and Discussion

3.1 Annual Cycle of LAI

The mean annual cycle of LAI from 1999 to 2015 is shown in figure 2 for the three experimental domains. The timing of the maximum LAI in the simulations is closest to

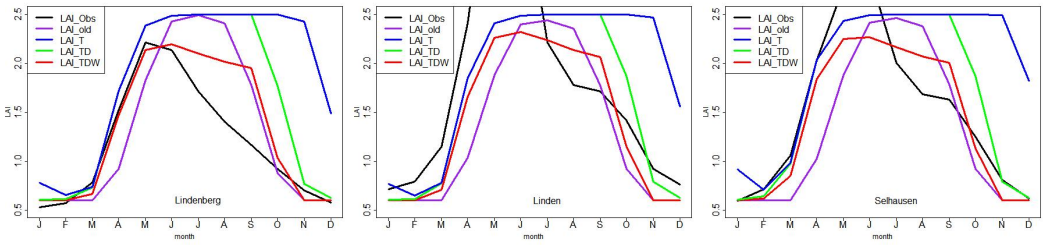

Figure 2. Mean (1999-2015) annual cycle of LAI. Results with the standard phenology(*_old*, –), with only the dependence on temperature implemented (*_T*, –), with the dependence on day length added (*_TD*, –), with the fully implemented new phenology (*_TDW*, –), and satellite observations (*_Obs*, –) are shown at the three experimental domains Lindenberg, Linden, and Selhausen.

observations with the newly implemented phenology. The maximum value of LAI of the standard simulations is reached in July whereas in the observations it is between May and June. Implementing the dependence on temperature, the LAI stays at maximum from June to November. Implementing additionally the dependence on day length, it follows the same mean annual cycle as with only the dependence on temperature except for the earlier decrease in September. At the end of the growing season, the day length threshold intervenes earlier than the temperature threshold. The water availability of the complete newly implemented phenology reduces the LAI in summer which is why the maximum value is between May and June, the same time of the year as in the observations. Also, the start of the growing season of the simulations with the newly implemented phenology is in very good agreement with the observations. This applies to all simulations except for those with the standard phenology. More details will follow in the next section. However, the decrease of LAI starts later and faster in the simulations compared to the observations but it ends at a similar time in the simulations (except for the simulation only depending on temperature) and the observations.

Two differences remain between the simulations with the new phenology and the observations (figure 2). The first one is the difference in the maximum value of LAI. It is higher in the observations of Linden and Selhausen than in the simulations. This is because the maximum value of LAI is fixed in the model through the external parameters. Another reason is that the satellite observations are related to different land-use classes like urban areas, agriculturally used areas, and grassland, whereas in the simulations all land-use classes are adjusted to grassland. The second difference between the observations and the simulations can be found with LAI values from July to October up to $1\,m^2/m^2$ higher in the simulations than in the observations. An explanation is the human impact through land use management. In Germany, the part of human used land (agricultural, settlement, and transport area) is more than 65 % (Umweltbundesamt, 2018). Humans cut grass and harvest crops during summer and early autumn. This is the period of the largest difference between the simulations and the observations in figure 2. The human activities reduce the LAI in the observations, but this cannot be simulated in CCLM because it is not a natural process. Those processes can not be represented even in sophisticated models (Davin et al., 2014).

Correlation coefficients r between simulations and the observations are calculated to evaluate the quality of the different simulations (table 2). Very high and significant correlations are found for all simulations at the three stations. The highest correlation coefficients are found between the simulations with the new phenology and the satellite observations, followed by the simulations with the dependence on temperature and day

Table 2. Pearson's correlation coefficient r for the monthly LAI of the different simulations from 1999 to 2015 compared to satellite observations, Fisher's z for Pearson's r of the standard simulation compared to the new phenology (in italic), and the p-value calculated from Fisher's z (significant in bold).

	r (LAI_ old∼Obs)	r (LAI_ T∼Obs)	r (LAI_ TD∼Obs)	r (LAI_ TDW∼Obs)	z (old∼ TDW)	p (Fisher)
Lindenberg	0.73	0.56	0.77	0.82	*-2.287*	***0.011***
Linden	0.67	0.51	0.71	0.77	*-2.101*	***0.018***
Selhausen	0.76	0.57	0.81	0.86	*-2.979*	***0.001***

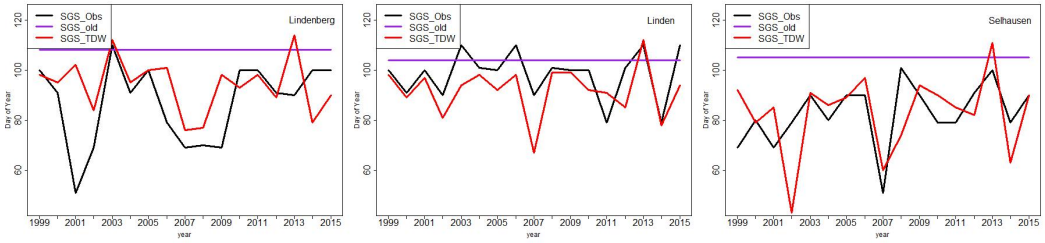

Figure 3. Start of the growing season (SGS) in number of days for each year from 1999 to 2015 and each domain (Lindenberg, Linden, and Selhausen) for satellite observations (*_Obs*, –), the standard phenology simulations (*_old*, –), and the new phenology simulations (*_TDW*, –).

length of the new phenology, the standard phenology, and finally, the phenology only depending on the temperature.

The improvement of the simulations compared to observations is quantified by Fisher's z. The values and their probabilities for the comparison of the new phenology to the old phenology are also shown in table 2. The improvement of the simulations from the standard to the new phenology is significant at all locations. More information to the statistical methods can be found in the appendix.

In summary, the mean annual satellite-observed cycle of LAI is represented most accurately in the model with the newly implemented phenology. The representation of LAI improved significantly compared to the standard phenology at all locations. In the following section, we analyze the start of the growing season (SGS) of each year.

Start of the Growing Season

The start of the growing season (SGS) is defined as the day when the LAI has reached 20 % of its maximum value (Murray-Tortarolo et al., 2013; Anav et al., 2013). In figure 3 the SGS is shown for the three domains in the satellite observations, the simulations with the standard phenology, and the simulations with the new phenology. In the simulations with the standard phenology, the SGS is constant because of the annually-recurring cycle. The observations as well as the new simulations, have a large interannual variability and are significantly positive correlated (Lindenberg $r = 0.27$, Linden $r = 0.64$, Selhausen $r = 0.45$). For the majority of the years, the SGS of the simulations with the standard phenology is approximately 2 months later compared to the observations and the simulations with the new phenology (figure 3). This is because the phenology in the standard simulation only depends on the latitude and altitude specifying the SGS at that

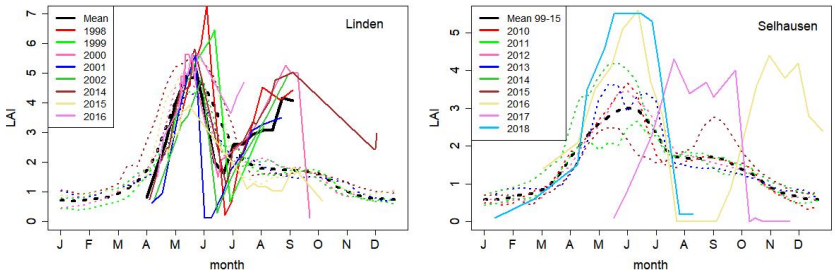

Figure 4. LAI satellite (dotted) and in-situ (lines) observations at Linden and Selhausen for the years shown in the legend on the left in different colors. In-situ measurements are only available for the given years and dates. At Linden, the shown simulated years are (except 1998) the same as the in-situ observations. At Selhausen, the six years of simulations before the in-situ observations are shown. The mean yearly cycle of the satellite LAI for the given years is shown in black (–).

date. When depending on temperature and day length in the new phenology module, the SGS is earlier in spring and therefore closer to the observations.

In summary, the simulations with the newly implemented phenology with the interannual variability of SGS show the most similarity with the observations from satellite data. The reliability of the satellite data is studied in the next section by comparing the data to in-situ measurements.

Validation of Observations

The stations Linden and Selhausen have in-situ measurements of the LAI. They can be used to validate the satellite data with less precise results at a specific location but constant horizontal and temporal resolution over a large domain and period (figure 4). The in-situ measurements of LAI at Linden have two peaks per year because the grass is cut twice a year. The first cutting is between the end of May and the beginning of June showing the first decrease of LAI. The second cut is in September associated with the second decrease of LAI. The satellite observation in the pixel including Linden shows the first peak of LAI and a slightly increased value during the second peak of the in-situ measurements. At Selhausen, the crops are harvested at a different time but only once each year, hence the differences in the in-situ measurements of LAI in figure 4. In the satellite observation over Selhausen, the first peak is nearly at the same time as over Linden. It can also be seen in the in-situ measurements (2016: barley, 2018: winter wheat). The second peak is also pronounced in the satellite observations but still with an only slightly increased signal. At the same time, the peak appears in the in-situ measurements of 2017 (sugar beet) and later in 2016 (greening mix).

The major peak of the mean satellite observed LAI (figure 4) is in very good agreement with the first peak of grass or the winter crops (e.g. barley, winter wheat) and the minor peak is in good agreement with the second growth of grass or the summer crops (e.g. sugar beet). That indicates a high percentage of human activities in the satellite observations (cutting of grass and harvesting) (figure 4). Those human-induced, not natural processes are not part of the model. Hence, figure 2 shows differences between the simulations and the observations. Differences in the annual cycle of LAI due to environmental conditions are dealt with in the next section.

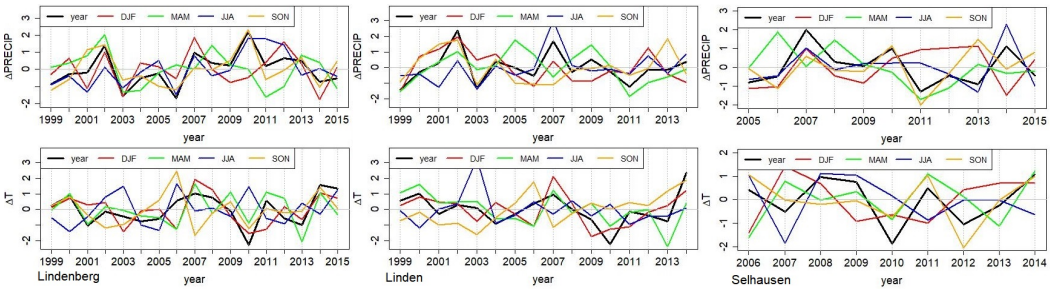

Figure 5. Standardized precipitation (top) and temperature (bottom) for each year of observations with the mean value in black, and the seasons winter (DJF, –), spring (MAM, –), summer (JJA, –), and autumn (SON, –) in different colors.

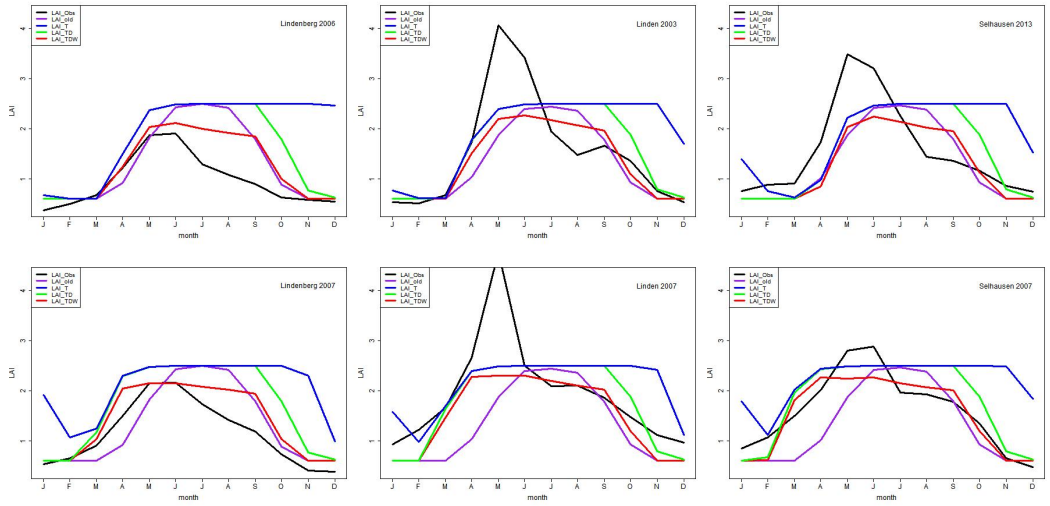

Figure 6. Annual cycle of LAI of the extremely dry years 2006 at Lindenberg, 2003 at Linden, and 2013 at Selhausen (top) and the year 2007 with extremely warm spring at Lindenberg, Linden, and Selhausen (bottom). In black (–) are the satellite observations (_Obs) and in different colors the simulations with the standard phenology (_old, –), with only the dependence on temperature (_T, –), the dependence on temperature and day length (_TD, –), and with the new phenology (_TDW, –).

Influence of Temperature and Precipitation Extremes

Figure 5 presents the standardized observed precipitation and temperature for the three experimental domains. The data is measured in-situ at different stations described in section 2.1. The drier the summer is the more the LAI is reduced due to water availability. The driest summers in figure 5 are 2006 at Lindenberg, 2003 at Linden and 2013 at Selhausen. The warmest winter and spring in figure 5 is 2007 at Lindenberg, Linden, and Selhausen. For the years with extreme events, the annual cycle of LAI is presented in figure 6. The satellite observations show a very sharp decrease in LAI during summer at all locations in the extremely dry years (upper panel of fig. 6). With the simulations including the dependence on water availability in red, the decrease of LAI starts at the same time as in the observations but is not as steep. The reduction due to water stress is improved compared to the simulations without dependence on water availability but is still limited by the thresholds. The improvement in the annual cycle of LAI of the ex-

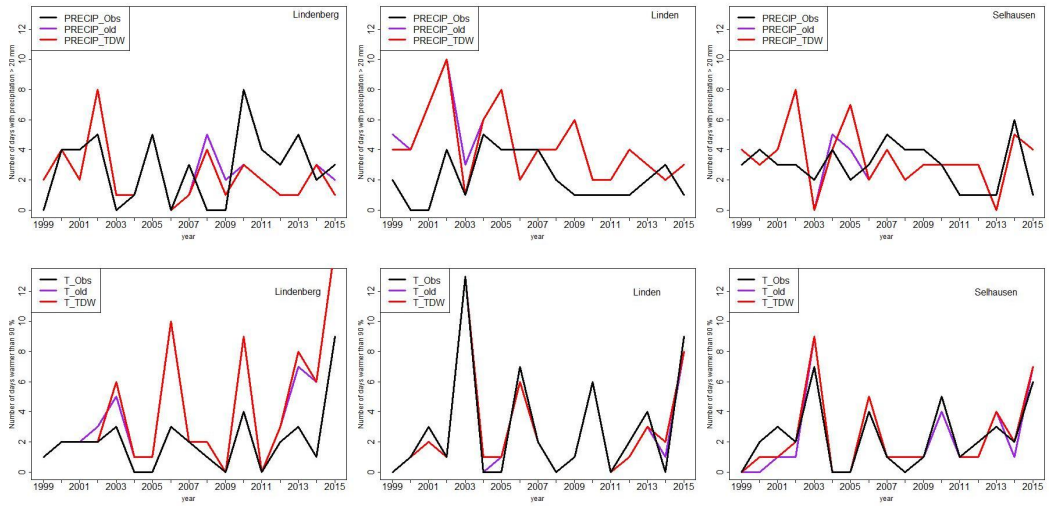

Figure 7. Heavy precipitation events with more than 20 mm per day (top) and very warm days within the 90 th Percentile of the observed maximum temperatures (bottom) in each year of the period 1999 to 2015 at Lindenberg, Linden and Selhausen for the HYRAS observations (_Obs, –), the simulations with the standard phenology (_old, –) and the simulations with the new phenology (_TDW, –).

treme year 2007 is shown in the lower panel of figure 6. The winter and spring of 2007 were exceptionally warm with a strong impact on Germany's phenology (Luterbacher et al., 2007). The early SGS shown in the satellite observations can be simulated with the newly implemented phenology because all simulations (_T, _TD, _TDW) show a clear dependence on temperature. The standard phenology only depends on the latitude and the altitude thus does not have an earlier SGS because of climatic conditions. Hence, the SGS in those years is about two months later (figure 6 and figure 3).

In summary, we show that extreme temperature and precipitation events are influencing the annual cycle of LAI. In contrast to simulations with the standard phenology module, CCLM can reproduce interannual variations in the annual cycle of the LAI with the newly implemented phenology depending on surface temperature, day length, and water availability.

3.2 Impacts of LAI

Impact on Precipitation and Temperature Extremes

The influence of phenology on extreme precipitation and temperature (the opposite of what was previously studied) is shown in figure 7. The simulations with the standard phenology and the new phenology are compared to the HYRAS gridded observational data set (Rauthe et al., 2013). Heavy precipitation events with more than 20 mm precipitation on one day are shown in the upper panel of figure 7. The number of heavy precipitation events is similar for all simulations and the observations at Lindenberg and Selhausen. At Linden, the simulations have, on average, twice as much heavy precipitation events as the observations. This could be due to the differences in land cover type between reality and the modified grassland in the simulations. The total number of heavy precipitation events in the simulations with the new phenology is closer to the observations in more years than with the standard phenology at Lindenberg and Linden and equal at Selhausen.

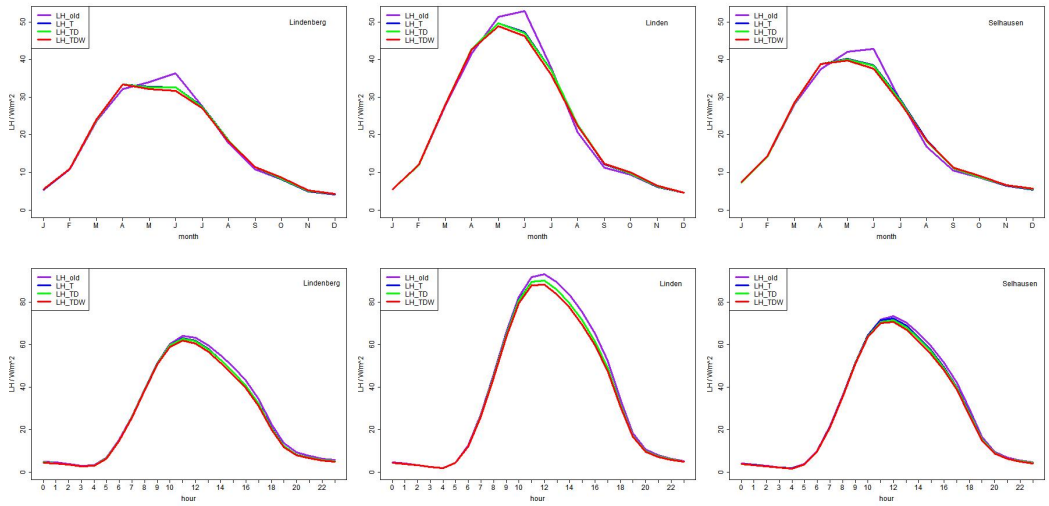

Figure 8. Mean (1999-2015) annual latent heat flux (top) and mean (1999-2015) daily latent heat flux during summer JJA (bottom) at Lindenberg, Linden and Selhausen for the simulations with the standard phenology (_old, –), with only the dependence on temperature (_T, –), the dependence on temperature and day length (_TD, –), and the simulations with the new phenology (_TDW, –).

The number of days within the 90 th percentile of the maximum temperatures per year can be seen in the bottom part of figure 7. The years with the most extreme warm days are the same in the simulations and the observations. The correlation coefficients r between the simulations and the observations are with 0.89 for Lindenberg up to 0.99 for Linden very high. For Lindenberg, the average total number of days in the simulations is twice as much as in the observations, again this may be due to the differences in land cover type between the reality and the simulations. The average number of days with the new phenology is generally closer to the observations than the number in the simulations with the old phenology. The number of years, where the number of extremely warm days fits better to the observations at Selhausen, is higher in the simulations with the new phenology (figure 7).

In summary, simulations with the new phenology are more realistic regarding extreme events in precipitation and temperature because they fit better to the HYRAS observations than the simulations with the standard phenology. The influence of phenology on the regional climate can also be seen in the transpiration, which is shown in the following section.

Impact on Latent Heat Flux

The vegetation also has a large impact on the latent heat flux due to transpiration. Figure 8 (upper panel) shows the mean annual cycle of latent heat flux for the simulations with different phenology calculations. In spring (March and April) and autumn (August to October) the latent heat flux of the simulations with the new phenology is a few W/m^2 higher. But in summer (May to July) the simulations with the old phenology are up to $5\,W/m^2$ higher on average.

In summer, when the differences between the models are highest, the mean daily cycle also differs. The lower panel of figure 8 shows the mean daily cycle of latent heat flux for all summer days (June, July, and August) and all simulated years for the three locations. The difference is highest during the daytime when the sun is at its zenith. Then

the influence of more vegetation in the simulations with the standard phenology is highest and transpires more what increases the latent heat flux. The simulations with the new phenology have the lowest latent heat flux values in summer because of less vegetation. During nighttime when there is no solar radiation the latent heat flux is very low.

The expected influence of vegetation on latent heat flux (Yang et al., 1999; Peñuelas et al., 2009) is shown in the simulations with the new phenology module. The latent heat flux in summer is reduced because the LAI is also reduced due to the dependence on water availability in the new phenology scheme. The lower LAI causes lower transpiration and lowers latent heat flux. This causes lower humidity in the atmosphere and therefore higher temperatures. The latent heat flux in summer is highest at Linden, followed by Selhausen and Lindenberg. In general, radiation, precipitation, the climate type of the area, and the vegetation type are found to be important factors for the evapotranspiration (C. Williams et al., 2012). The type of vegetation and the climate type are predefined in the simulations and the same at the three domains. Precipitation is highest at Selhausen, followed by Linden and Lindenberg. This influences low latent heat fluxes at Lindenberg. Radiation creates the remaining differences.

In summary, the influence of the phenology on the energy and water fluxes is shown by the comparison of the latent heat flux simulated with the standard phenology and with the newly implemented phenology. As expected, less vegetation in summer with the new phenology leads to less latent heat. This also influences the representation of all related variables like humidity and temperature.

4 Conclusion

In this study, a new implementation of phenology in the COSMO-CLM model is presented. The LAI as an indicator for phenology is calculated in the new module depending on surface temperature, day length, and water availability. Simulations are performed at three locations in Germany (Lindenberg, Linden, and Selhausen) from 1999 to 2015 with the standard phenology, with phenology depending on temperature, depending on temperature and day length and with the complete new phenology. The results of the simulations with different calculation methods of LAI were compared with each other and with observations. The questions in the introduction can be answered as follows:

1. How is the annual cycle of LAI affected by the newly implemented phenology?
   The representation of the annual cycle of LAI significantly improved using the newly implemented phenology compared to the standard phenology in CCLM. The timing of LAI including its increase, maximum, and decrease is closer to observations with the new simulations. The interannual variability of the simulated SGS is more consistent with the observations.
2. Does the representation of extreme events in CCLM change with the new phenology module?
   Extreme warm/dry years and their influence on phenology can be better resolved with the new phenology in CCLM. The previously static annual cycle of LAI is adjusted with the dependence on temperature and water availability to extreme environmental conditions. On the other hand, the higher variability of LAI of the newly implemented phenology shows a better representation of extreme precipitation and temperature events compared to the standard simulations with the annually-recurring phenology. The number of heavy precipitation events per year and the average number of extremely warm days have been improved.
3. What is the influence of the phenology on atmospheric variables, such as temperature, precipitation, and moisture?
   The newly implemented phenology causes changes in the energy and water cycle of the model compared to the standard simulations. Lower LAI values (less vegetation) with the new phenology lead to less transpiration and latent heat flux,

resulting generally in lower humidity and higher temperature. Those differences are small but especially in extreme years with less available water and higher temperatures they are associated with a stronger positive feedback mechanism which leads to less water and higher temperatures. The model with the standard phenology does not show the interannual differences and therefore misses this effect.

The additional computational costs of the new phenology module are negligible and it can be implemented easily. Considering this and the significant improvement it achieves, the new phenology module will constitute a significant advance for CCLM. The newly implemented phenology has interannual variability, which reveals changes in vegetation due to climate change. The opposite effect of changes in phenology on climate change can also be seen. Both processes are very important for predicting future climate change with CCLM.

In summary, the LAI of the model, especially in summer, still needs enhancement because the observations are highly influenced by human impact on vegetation (cutting of grass, harvesting). Those human interventions in nature are not simulated in CCLM and can therefore not be seen in the results. The next step is to simulate the phenology for different vegetation types like deciduous and evergreen forest, summer and winter crop over a larger domain in Central Europe.

Appendix A Statistical Methods

A1 Pearson Correlation

The pearson correlation coefficient or Pearson's r is used to measure the correlation between two variables x and y (Pearson & Filon, 1898). It has values between +1 and -1 with $r = 1$ means total positive linear correlation, $r = 0$ means no linear correlation, and $r = -1$ means total negative linear correlation. Pearson's r is calculated with

$$r = \frac{\mathrm{cov}(x, y)}{\sigma_x \sigma_y} \,. \tag{A1}$$

cov is the covariance of the two respective variables and σ_x and σ_y are the standard deviations. When comparing simulation results to observations the correlation is best the closer r is to 1.

A2 Fisher Transformation

The Fisher transformation is used to compare two different pearson correlation coefficients (Fisher, 1925). With calculating z the relation of the different r values can be estimated as follows

$$z = \frac{1}{2} \ln \left(\frac{1 + r}{1 - r} \right) \,. \tag{A2}$$

The probability p that the two correlations are related can be calculated with the confidence interval around the Fisher's z (Eid et al., 2017). The smaller p the higher is the probability that the two correlations are not related. This means if $p < 0.05$ the difference is significant if $p < 0.01$ the difference is very significant and if $p < 0.001$ the difference is highly significant.

A3 Standardization

The standardization is used to find the values that differ most from the average. The standardized form z of a variable x is calculated as

$$z(x) = \frac{x - \mu}{\sigma} \,, \tag{A3}$$

with the mean μ and the standard deviation σ. The higher the absolute value of z the more extreme is the variable x.

Acronyms

CCLM COSMO-CLM
DWD German Meteorological Service (Deutscher Wetterdienst)
LAI Leaf Area Index
SGS Start of Growing Season

Acknowledgments

The authors acknowledge the German Meteorological Service (DWD) for providing observational data at the DWD Climate Data Center (CDC) and the HYRAS data. The SPOT/PROBA-V LAI data product was generated by the land service of Copernicus, the Earth Observation programme of the European Commission. The research leading to the current version of the LAI product has received funding from various European Commission Research and Technical Development programmes. The product is based on SPOT/VGT 1km data ((c) CNES / PROBA-V 1km data ((c) ESA and distributed by VITO), last access date: 28/9/2018. We acknowledge the GiFACE project at Linden for producing the LAI and meteorological data at the Justus-Liebig-University Gießen. We would like to thank the IBG-3 of the Forschungszentrum Jülich for providing us with measurement data collected in the framework of the Transregional Collaborative Research Center 32 (DFG) and the HGF initiative TERestrial ENvironmental Observations (TERENO). Computational resources were made available by the German Climate Computing Center (DKRZ) through support from the Federal Ministry of Education and Research in Germany (BMBF). We acknowledge the funding of the German Research Foundation (DFG) through grant nr. 401857120.

References

Anav, A., Murray-Tortarolo, G., Friedlingstein, P., Sitch, S., Piao, S., & Zhu, Z. (2013). Evaluation of land surface models in reproducing satellite Derived leaf area index over the high-latitude northern hemisphere. Part II: Earth system models. *Remote Sensing*, *5*(8), 3637–3661.

Andresen, L. C., Yuan, N., Seibert, R., Moser, G., Kammann, C. I., Luterbacher, J., ... Müller, C. (2018). Biomass responses in a temperate European grassland through 17 years of elevated CO2. *Global Change Biology*, *24*(9), 3875–3885.

Baldauf, M., Seifert, A., Förstner, J., Majewski, D., Raschendorfer, M., & Reinhardt, T. (2011). Operational convective-scale numerical weather prediction with the COSMO model: description and sensitivities. *Monthly Weather Review*, *139*(12), 3887–3905.

Baret, F., Weiss, M., Lacaze, R., Camacho, F., Makhmara, H., Pacholcyzk, P., & Smets, B. (2013). GEOV1: LAI and FAPAR essential climate variables and FCOVER global time series capitalizing over existing products. Part1: Principles of development and production. *Remote sensing of environment*, *137*, 299–309.

Bartholy, J., & Pongrácz, R. (2007). Regional analysis of extreme temperature and precipitation indices for the Carpathian Basin from 1946 to 2001. *Global and Planetary change*, *57*(1-2), 83–95.

Best, M., & Grimmond, C. (2016). Modeling the partitioning of turbulent fluxes at urban sites with varying vegetation cover. *Journal of Hydrometeorology*, *17*(10), 2537–2553.

Bogena, H., Montzka, C., Huisman, J., Graf, A., Schmidt, M., Stockinger, M., ... Vereecken, H. (2018). The TERENO-Rur Hydrological Observatory: A multi-scale multi-compartment research platform for the advancement of hydrological science. *Vadose Zone Journal*, *17*(1).

Camacho, F., Cernicharo, J., Lacaze, R., Baret, F., & Weiss, M. (2013). GEOV1: LAI, FAPAR essential climate variables and FCOVER global time series capitalizing over existing products. Part 2: Validation and intercomparison with reference products. *Remote Sensing of Environment*, *137*, 310–329.

Chen, J., Menges, C., & Leblanc, S. (2005). Global mapping of foliage clumping index using multi-angular satellite data. *Remote Sensing of Environment*, *97*(4), 447–457.

Chmielewski, F.-M., & Rötzer, T. (2002). Annual and spatial variability of the beginning of growing season in Europe in relation to air temperature changes. *Climate research*, *19*(3), 257–264.

Collatz, G. J., Bounoua, L., Los, S., Randall, D., Fung, I., & Sellers, P. (2000). A mechanism for the influence of vegetation on the response of the diurnal temperature range to changing climate. *Geophysical Research Letters*, *27*(20), 3381–3384.

Currie, P. O., & Peterson, G. (1966). Using growing-season precipitation to predict crested wheatgrass yields. *Journal of Range Management*, 284–288.

Cutini, A., Matteucci, G., & Mugnozza, G. S. (1998). Estimation of leaf area index with the Li-Cor LAI 2000 in deciduous forests. *Forest Ecology and Management*, *105*(1-3), 55–65.

Davin, E. L., Seneviratne, S. I., Ciais, P., Olioso, A., & Wang, T. (2014). Preferential cooling of hot extremes from cropland albedo management. *Proceedings of the National Academy of Sciences*, *111*(27), 9757–9761.

Dee, D. P., Uppala, S. M., Simmons, A. J., Berrisford, P., Poli, P., Kobayashi, S., ... Vitart, F. (2011). The ERA-Interim reanalysis: Configuration and performance of the data assimilation system. *Quarterly Journal of the royal meteorological society*, *137*(656), 553–597.

Dickinson, R. E. (1984). Modeling evapotranspiration for three-dimensional global climate models. *Climate processes and climate sensitivity*, *29*, 58–72.

Doms, G., Förstner, J., Heise, E., Herzog, H., Mironov, D., Raschendorfer, M., ... Vogel, G. (2011). A Description of the Nonhydrostatic Regional COSMO Model. Part II: Physical parameterization. *Deutscher Wetterdienst, Offenbach, Germany*. (Available at http://www.cosmo-model.org/)

Eid, M., Gollwitzer, M., & Schmitt, M. (2017). *Statistik und Forschungsmethoden : mit Online-Materialien* (Vol. 5). Weinheim; Basel : Beltz, 2017.

Fisher, R. A. (1925). *Statistical methods for research workers* (Vol. 6). Oliver and Boyd, Edinburgh, Scotland.

Flerchinger, G., Kustas, W., & Weltz, M. (1998). Simulating surface energy fluxes and radiometric surface temperatures for two arid vegetation communities using the SHAW model. *Journal of Applied Meteorology*, *37*(5), 449–460.

Gardner, W., & Ehlig, C. (1963). The influence of soil water on transpiration by plants. *Journal of Geophysical Research*, *68*(20), 5719–5724.

Gilgen, A. K., & Buchmann, N. (2009). Response of temperate grasslands at different altitudes to simulated summer drought differed but scaled with annual precipitation. *Biogeosciences Discussions*, *6*(3), 5217–5250.

Giorgetta, M. A., Jungclaus, J., Reick, C. H., Legutke, S., Bader, J., Böttinger, M., ... Stevens, B. (2013). Climate and carbon cycle changes from 1850 to 2100 in MPI-ESM simulations for the Coupled Model Intercomparison Project phase 5. *Journal of Advances in Modeling Earth Systems*, *5*(3), 572–597.

González-Aparicio, I., & Hidalgo, J. (2012). Dynamically based future daily and seasonal temperature scenarios analysis for the northern Iberian Peninsula. *International journal of climatology*, *32*(12), 1825–1833.

Heide, O. M. (1974). Growth and dormancy in Norway spruce ecotypes (Picea abies) I. Interaction of photoperiod and temperature. *Physiologia Plantarum*, *30*(1), 1–12.

Hodges, T. (1991). Temperature and water stress effects on phenology. *Predicting*

crop phenology, 7–13.

Jacob, D., & Podzun, R. (1997). Sensitivity studies with the regional climate model REMO. *Meteorology and Atmospheric Physics*, *63*(1-2), 119–129.

Jameson, A., Schmidt, W., & Turkel, E. (1981). Numerical solution of the Euler equations by finite volume methods using Runge Kutta time stepping schemes. In *FLUID MECHANICS AND HEAT TRANSFER.* United States: NASA Center for Aerospace Information (CASI).

Jarvis, P. (1976). The interpretation of the variations in leaf water potential and stomatal conductance found in canopies in the field. *Philosophical Transactions of the Royal Society of London. B, Biological Sciences*, *273*(927), 593–610.

Jeong, S.-J., HO, C.-H., GIM, H.-J., & Brown, M. E. (2011). Phenology shifts at start vs. end of growing season in temperate vegetation over the Northern Hemisphere for the period 1982–2008. *Global change biology*, *17*(7), 2385–2399.

Jäger, H., Schmidt, S., Kammann, C., Grünhage, L., Müller, C., & Hanewald, K. (2003). The University of Giessen Free-Air Carbon Dioxide Enrichment study: Description of the experimental site and of a new enrichment system. *Journal of Applied Botany*, *77*(5-6), 117-127.

Kammann, C., Grunhage, L., Gruters, U., Janze, S., & Jager, H. (2005). Response of aboveground grassland biomass and soil moisture to moderate long-term CO2 enrichment. *Basic and Applied Ecology*, *6*(4), 351-365.

Knorr, W., Kaminski, T., Scholze, M., Gobron, N., Pinty, B., Giering, R., & Mathieu, P.-P. (2010). Carbon cycle data assimilation with a generic phenology model. *Journal of Geophysical Research: Biogeosciences*, *115*(G4).

Kundzewicz, Z. W., Radziejewski, M., & Pinskwar, I. (2006). Precipitation extremes in the changing climate of Europe. *Climate Research*, *31*(1), 51–58.

Li-Cor, I. (1992). LAI-2000 plant canopy analyzer instruction manual. *LI-COR Inc., Lincoln, Nebraska, USA*.

Luterbacher, J., Liniger, M. A., Menzel, A., Estrella, N., Della-Marta, P. M., Pfister, C., ... Xoplaki, E. (2007). Exceptional European warmth of autumn 2006 and winter 2007: Historical context, the underlying dynamics, and its phenological impacts. *Geophysical Research Letters*, *34*(12).

Manabe, S. (1969). Climate and the ocean circulation: I. The atmospheric circulation and the hydrology of the earth's surface. *Monthly Weather Review*, *97*(11), 739–774.

Menzel, A., & Fabian, P. (1999). Growing season extended in europe. *NATURE*, *397*(6721), 659.

Merkel, A. O. P. A. (2020). *climate-data.org.* Retrieved 13.02.2020, from `https://de.climate-data.org/europa/deutschland/`

Murray-Tortarolo, G., Anav, A., Friedlingstein, P., Sitch, S., Piao, S., Zhu, Z., ... Zeng, N. (2013). Evaluation of land surface models in reproducing satellite-derived LAI over the high-latitude Northern Hemisphere. Part I: Uncoupled DGVMs. *Remote Sensing*, *5*(10), 4819–4838.

Nagai, H. (2003). Validation and sensitivity analysis of a new atmosphere–soil–vegetation model. Part II: Impacts on in-canopy latent heat flux over a winter wheat field determined by detailed calculation of canopy radiation transmission and stomatal resistance. *Journal of Applied Meteorology*, *42*(3), 434–451.

Neisser, J., Adam, W., Beyrich, F., Leiterer, U., & Steinhagen, H. (2002). Atmospheric boundary layer monitoring at the Meteorological Observatory Lindenberg as a part of the "Lindenberg Column": Facilities and selected results. *Meteorologische Zeitschrift*, *11*(4), 241–253.

Oleksyn, J., Tjoelker, M., & Reich, P. B. (1992). Growth and biomass partitioning of populations of European Pinus sylvestris L. under simulated 50° and 60°N daylengths: evidence for photoperiodic ecotypes. *New Phytologist*, *120*(4), 561–574.

Oleson, K., Lawrence, D., Bonan, G., Drewniak, B., Huang, M., Koven, C., ... Yang, Z.-L. (2013). *Technical description of version 4.5 of the Community Land Model (CLM).* (Available at http://www.cesm.ucar.edu/)

Parmesan, C. (2006). Ecological and evolutionary responses to recent climate change. *Annual Review of Ecology Evolution and Systematics*, *37*, 637-669.

Parmesan, C., & Yohe, G. (2003). A globally coherent fingerprint of climate change impacts across natural systems. *NATURE*, *421*(6918), 37-42.

Pearson, K., & Filon, L. N. G. (1898). VII. Mathematical contributions to the theory of evolution.—IV. On the probable errors of frequency constants and on the influence of random selection on variation and correlation. *Philosophical Transactions of the Royal Society of London. Series A, Containing Papers of a Mathematical or Physical Character*(191), 229–311.

Peñuelas, J., Rutishauser, T., & Filella, I. (2009). Phenology feedbacks on climate change. *Science*, *324*(5929), 887–888.

Piao, S., Tan, J., Chen, A., Fu, Y., Ciais, P., Liu, Q., ... Penuelas, J. (2015). Leaf onset in the northern hemisphere triggered by daytime temperature. *Nature Communications*, *6*, 6911.

Post, H., Hendricks Franssen, H.-J., Han, X., Baatz, R., Montzka, C., Schmidt, M., & Vereecken, H. (2018). Evaluation and uncertainty analysis of regional-scale CLM4. 5 net carbon flux estimates. *Biogeosciences*, *15*(1), 187–208.

Raddatz, T., Reick, C., Knorr, W., Kattge, J., Roeckner, E., Schnur, R., ... Jungclaus, J. (2007). Will the tropical land biosphere dominate the climate–carbon cycle feedback during the twenty-first century? *Climate Dynamics*, *29*(6), 565–574.

Rauthe, M., Steiner, H., Riediger, U., Mazurkiewicz, A., & Gratzki, A. (2013). A Central European precipitation climatology–Part I: Generation and validation of a high-resolution gridded daily data set (HYRAS). *Meteorologische Zeitschrift*, *22*(3), 235–256.

Reick, C., Raddatz, T., Brovkin, V., & Gayler, V. (2013). Representation of natural and anthropogenic land cover change in MPI-ESM. *Journal of Advances in Modeling Earth Systems*, *5*(3), 459–482.

Reyes-Fox, M., Steltzer, H., Trlica, M., McMaster, G. S., Andales, A. A., LeCain, D. R., & Morgan, J. A. (2014). Elevated CO2 further lengthens growing season under warming conditions. *NATURE*, *510*(7504), 259–262.

Richardson, A. D., Keenan, T. F., Migliavacca, M., Ryu, Y., Sonnentag, O., & Toomey, M. (2013). Climate change, phenology, and phenological control of vegetation feedbacks to the climate system. *Agricultural and Forest Meteorology*, *169*, 156–173.

Rockel, B., Will, A., & Hense, A. (2008). The regional climate model COSMO-CLM (CCLM). *Meteorologische Zeitschrift*, *17*(4), 347–348.

Ryder, J., Polcher, J., Peylin, P., Ottle, C., Chen, Y.-Y., van Gorsel, E., ... Luyssaert, S. (2014). A multi-layer land surface energy budget model for implicit coupling with global atmospheric simulations. *Geoscientific Model Development Discussions*, *7*(1), 8649–8701.

Schnelle, F. (1955). *Pflanzen-Phänologie.* Akademische Verlagsgesellschaft Geest & Portig, Leipzig.

Schättler, U., & Blahak, U. (2017). A Description of the Nonhydrostatic Regional COSMO-Model. Part V: Preprocessing: Initial and Boundary Data for the COSMO-Model. *Deutscher Wetterdienst, Offenbach, Germany*. (Available at http://www.cosmo-model.org/)

Schulz, J.-P., Vogel, G., & Ahrens, B. (2015). A new leaf phenology for the land surface scheme TERRA of the COSMO atmospheric model. *COSMO Newsletter*, *15*. (Available at http://www.cosmo-model.org/)

Schulz, J.-P., Vogel, G., Becker, C., Kothe, S., Rummel, U., & Ahrens, B. (2016). Evaluation of the ground heat flux simulated by a multi-layer land surface

scheme using high-quality observations at grass land and bare soil. *Meteorologische Zeitschrift*, *25*(5), 607–620.

Settele, J., Scholes, R., Betts, R., Bunn, S., Leadley, P., Nepstad, D., ... Taboad, M. (2014). *Terrestrial and inland water systems. In: Climate Change 2014: Impacts, Adaptation, and Vulnerability. Part A: Global and Sectoral Aspects. Contribution of Working Group II to the Fifth Assessment Report of the Intergovernmental Panel on Climate Change* (C. Field et al., Eds.). Cambridge University Press, Cambridge, United Kingdom and New York, NY, USA. (pp. 271-359)

Shen, M., Tang, Y., Chen, J., Zhu, X., & Zheng, Y. (2011). Influences of temperature and precipitation before the growing season on spring phenology in grasslands of the central and eastern Qinghai-Tibetan Plateau. *Agricultural and Forest Meteorology*, *151*(12), 1711–1722.

Sitch, S., Smith, B., Prentice, I., Arneth, A., Bondeau, A., Cramer, W., ... Venevsky, S. (2003). Evaluation of ecosystem dynamics, plant geography and terrestrial carbon cycling in the LPJ dynamic global vegetation model. *Global Change Biology*, *9*(2), 161–185.

Smets, B., Verger, A., Camacho, F., Van der Goten, R., & Jacobs, T. (2019). Copernicus Global Land Operations "Vegetation and Energy", PRODUCT USER MANUAL. *Issue 1.33 - version 2*. (Available at https://land.copernicus.eu/)

Smith, B., Prentice, I. C., & Sykes, M. T. (2001). Representation of vegetation dynamics in the modelling of terrestrial ecosystems: comparing two contrasting approaches within European climate space. *Global Ecology and Biogeography*, *10*(6), 621–637.

Stéfanon, M., Drobinski, P., d'Andrea, F., & de Noblet-Ducoudré, N. (2012). Effects of interactive vegetation phenology on the 2003 summer heat waves. *Journal of Geophysical Research: Atmospheres*, *117*(D24).

Tiedtke, M. (1988). Parameterization of cumulus convection in large-scale models. In *Physically-based modelling and simulation of climate and climatic change* (pp. 375–431). Springer.

Tölle, M. H., Gutjahr, O., Busch, G., & Thiele, J. C. (2014). Increasing bioenergy production on arable land: Does the regional and local climate respond? Germany as a case study. *Journal of Geophysical Research: Atmospheres*, *119*(6), 2711–2724.

Umweltbundesamt. (2018). *Umwelt und Landwirtschaft 2018.*

Verger, A., Baret, F., & Weiss, M. (2014). Near real-time vegetation monitoring at global scale. *IEEE Journal of Selected Topics in Applied Earth Observations and Remote Sensing*, *7*(8), 3473–3481.

Walther, G., Post, E., Convey, P., Menzel, A., Parmesan, C., Beebee, T., ... Bairlein, F. (2002). Ecological responses to recent climate change. *NATURE*, *416*(6879), 389-395.

Watson, D. J. (1947). Comparative physiological studies on the growth of field crops: I. Variation in net assimilation rate and leaf area between species and varieties, and within and between years. *Annals of botany*, *11*(41), 41–76.

White, M., Thornton, P., & Running, S. (1997). A continental phenology model for monitoring vegetation responses to interannual climatic variability. *Global Biogeochemical Cycles*, *11*(2), 217-234.

Wilhelm, C., Rechid, D., & Jacob, D. (2013). Dynamic coupling of regional atmosphere to biosphere in the new generation regional climate system model REMO-iMOVE. *Geoscientific Model Development Discussions*, *6*, 3085–3135.

Williams, C., Reichstein, M., Buchmann, N., Baldocchi, D., Beer, C., Schwalm, C., ... Schaefer, K. (2012). Climate and vegetation controls on the surface water balance: Synthesis of evapotranspiration measured across a global network of flux towers. *Water Resources Research*, *48*(6).

Williams, I. N., & Torn, M. S. (2015). Vegetation controls on surface heat flux par-

titioning, and land-atmosphere coupling. *Geophysical Research Letters*, *42*(21), 9416–9424.

Woodward, F. I. (1987). *Climate and plant distribution.* Cambridge University Press.

Yan, Z., Jones, P., Davies, T., Moberg, A., Bergstrom, H., Camuffo, D., ... Yang, C. (2002). Trends of extreme temperatures in Europe and China based on daily observations. *Climatic Change*, *53*, 355–392.

Yang, Z.-L., Dai, Y., Dickinson, R. E., & Shuttleworth, W. J. (1999). Sensitivity of ground heat flux to vegetation cover fraction and leaf area index. *Journal of Geophysical Research: Atmospheres*, *104*(D16), 19505–19514.